International Journal of Nanomedicine

Dovepress
open access to scientific and medical research

Open Access Full Text Article

ORIGINAL RESEARCH

^{68}Ga-radiolabeled bombesin-conjugated to trimethyl chitosan-coated superparamagnetic nanoparticles for molecular imaging: preparation, characterization and biological evaluation

This article was published in the following Dove Medical Press journal:
International Journal of Nanomedicine

Maliheh Hajiramezanali,[1] Fatemeh Atyabi,[2,3] Mona Mosayebnia,[1] Mehdi Akhlaghi,[4] Parham Geramifar,[4] Amir Reza Jalilian,[4] Seyed Mohammad Mazidi,[5] Hassan Yousefnia,[6] Soraya Shahhosseini,[7] Davood Beiki[4]

[1]Department of Radiopharmacy, Faculty of Pharmacy, Tehran University of Medical Sciences, Tehran, Iran; [2]Department of Pharmaceutical Nanotechnology, Faculty of Pharmacy, Tehran University of Medical Sciences, Tehran, Iran; [3]Nanotechnology Research Centre, Faculty of Pharmacy, Tehran University of Medical Sciences, Tehran, Iran; [4]Research Center for Nuclear Medicine, Shariati Hospital, Tehran University of Medical Sciences, Tehran, Iran; [5]Radiation Application Research School, Nuclear Science and Technology Research Institute (NSTRI), Tehran, Iran; [6]Material and Nuclear Fuel Research School, Nuclear Science and Technology Research Institute (NSTRI), Tehran, Iran; [7]Department of Radiopharmacy and Pharmaceutical Chemistry, School of Pharmacy, Shahid Beheshti University of Medical Sciences, Tehran, Iran

Correspondence: Fatemeh Atyabi
Nanotechnology Research Center, Faculty of Pharmacy, Tehran University of Medical Sciences, Tehran 1417614411, Iran
Tel +98 21 6695 9052
Email atyabifa@tums.ac.ir

Davood Beiki
Research Center for Nuclear Medicine, Shariati Hospital, Tehran University of Medical Sciences, North Kargar Avenue, Tehran, 14117113135, Iran
Tel +98 21 8802 6901
Email beikidav@tums.ac.ir

Introduction: Nowadays, nanoparticles (NPs) have attracted much attention in biomedical imaging due to their unique magnetic and optical characteristics. Superparamagnetic iron oxide nanoparticles (SPIONs) are the prosperous group of NPs with the capability to apply as magnetic resonance imaging (MRI) contrast agents. Radiolabeling of targeted SPIONs with positron emitters can develop dual positron emission tomography (PET)/MRI agents to achieve better diagnosis of clinical conditions.

Methods: In this work, *N*,*N*,*N*-trimethyl chitosan (TMC)-coated magnetic nanoparticles (MNPs) conjugated to *S*-2-(4-isothiocyanatobenzyl)-1,4,7,10-tetraazacyclododecane tetraacetic acid (DOTA) as a radioisotope chelator and bombesin (BN) as a targeting peptide (DOTA–BN–TMC–MNPs) were prepared and validated using fourier transform infrared (FTIR) spectroscopy, transmission electron microscopy (TEM), thermogravimetric analysis (TGA), vibrating sample magnetometer (VSM), and powder X-ray diffraction (PXRD) tests. Final NPs were radiolabeled with gallium-68 (^{68}Ga) and evaluated in vitro and in vivo as a potential PET/MRI probe for breast cancer (BC) detection.

Results: The DOTA–BN–TMC–MNPs with a particle size between 20 and 30 nm were efficiently labeled with ^{68}Ga (radiochemical purity higher than 98% using thin layer chromatography (TLC)). The radiolabeled NPs showed insignificant toxicity (>74% cell viability) and high affinity (IC_{50}=8.79 µg/mL) for the gastrin-releasing peptide (GRP)-avid BC T-47D cells using competitive binding assay against ^{99m}Tc–hydrazinonicotinamide (HYNIC)–gamma-aminobutyric acid (GABA)–BN (7–14). PET and MRI showed visible uptake of NPs by T-47D tumors in xenograft mouse models.

Conclusion: ^{68}Ga–DOTA–BN–TMC–MNPs could be a potential diagnostic probe to detect BC using PET/MRI technique.

Keywords: superparamagnetic iron oxide nanoparticles, trimethyl chitosan, bombesin, gallium-68, PET/MRI

Introduction

Nanoparticles (NPs) are considered as adjustable tools in biology and medicine as targeted drug delivery systems, biosensors, therapeutic and bioimaging agents because of their relatively large modifiable surface area, multimodal imaging properties, and multivalent interactions that increase affinity and residence time to their target.[1,2] NPs are being studied as targeted imaging agents due to their unique characteristics such as intrinsic magnetic and optical properties of superparamagnetic iron oxide

submit your manuscript | www.dovepress.com
Dovepress
http://dx.doi.org/10.2147/IJN.S195223

nanoparticles (SPIONs) and quantum dots, the potential for conjugation of targeting agents, and the capability to load the diagnostic moieties.[3,4]

SPIONs are biocompatible NPs that have attracted enormous attention as magnetic resonance imaging (MRI) contrast agents in clinical trials.[5,6] Multifunctional iron oxide NPs as multimodal imaging agents (positron emission tomography [PET]/MRI, single-photon emission computed tomography [SPECT]/MRI, optical/MRI contrast agents) can be utilized to overcome the limitations of single imaging modalities. The magnetic properties of SPIONs have also developed interesting therapeutic features including magnetic targeted drug delivery and hyperthermia. Such theranostic nanocarriers can improve diagnosis, treatment approaches by targeted therapy, and monitor therapeutic localization noninvasively.[7,8] In biomedical applications, the surface of SPIONs is usually modified by coating with different materials (eg, polyethylene glycol, dextran, and oleic acid) in order to enhance their biocompatibility and stability in aqueous solutions and supply functional groups for conjugation of anticancer drugs or targeting agents.[9,10] Chitosan is a versatile linear biopolymer studied in a variety of biomedical applications such as tissue engineering, drug/gene delivery, and molecular imaging due to its characteristics including biocompatibility, biodegradability, and low immunogenicity.[11,12] Chitosan solubility only in acidic media is the main limitation in applying chitosan for biomedical applications. *N*,*N*,*N*-trimethyl chitosan (TMC) is a water-soluble derivative of chitosan with a variety of biomedical applications such as tissue engineering and drug or gene delivery.[13,14] TMC as a cationic polymer can be applied as a coating layer for SPIONs to increase the stability of NPs in aqueous media and conjugate targeting ligands, drugs, and imaging agents for targeted therapy or diagnostic applications.

Breast cancer (BC) is a lethal commonly diagnosed malignancy in women worldwide, and early detection of BC is the most important strategy to treat the disease easily. Molecular imaging modalities including whole-body 2-deoxy-2-^{18}F-fluoro-D-glucose (^{18}F-FDG) PET/computed tomography (CT) and positron emission mammography (PEM) have been evaluated for primary BC diagnosis, staging, and monitoring the response to therapy.[15]

For years, the combination of PET and CT has offered concurrent anatomic and functional information in oncological imaging. In recent years, the integration of PET and MRI into a hybrid system has merged high sensitivity and metabolic characterization of PET with superior soft tissue characterization of MRI. Thus, it is necessary to develop the new radiolabeled contrast agents for PET/MRI.[16]

Radiolabeling of SPIONs with positron emitters can develop PET/magnetic resonance (MR) dual imaging probes.[17] Gallium-68 (^{68}Ga; $t_{1/2}$ 67.7 minutes, 89% β^+) is an attractive positron emitter radionuclide produced by ^{68}Ge/^{68}Ga generator as a continuous source of ^{68}Ga in hospitals. Several ^{68}Ga radiopharmaceuticals such as ^{68}Ga-labeled peptides and antibody fragments for targeted imaging of tumors have been developed and ^{68}Ga–DOTATATE is the first US Food and Drug Administration (FDA)-approved radiopharmaceutical to locate somatostatin receptor-positive neuroendocrine tumors, and the number is increasing in EU.

There are several specific biomarkers for targeted imaging of BC. Gastrin-releasing peptide (GRP) receptors are overexpressed in a variety of tumors including BC, small cell lung cancer, and prostate cancer.[18,19] Based on in vitro experiments, GRP receptors were found in many kinds of BC specimens, suggesting valuable opportunity for targeted imaging and/or therapy of BC.[20]

The amphibian analog of the GRP is bombesin (BN) with a high affinity to GRP receptors.[21] Radiolabeled BN derivatives have been applied to detect BC in early stages using SPECT and PET techniques.[22] BN analogs are a group of peptides used for active targeting of NPs to specifically bind to GRP receptors on the surface of cancer cells.[23]

The aim of the present study was to prepare the TMC-coated SPIONs conjugated to BN derivative and *S*-2-(4-isothiocyanatobenzyl)-1,4,7,10-tetraazacyclododecane tetraacetic acid (p-SCN-Bn-DOTA) followed by radiolabeling with ^{68}Ga for ultimate in vitro and in vivo evaluation in BC as a promising agent (Figure 1).

Materials and methods

Chitosan (110–150 kDa, 95% degree of deacetylation) was provided by Primex (Karmøy, Norway). All chemicals, reagents, and solvents were of analytical grade and were used without further purification. Succinyl–$(Gly)_8$–BN (7–14) with the sequence of succinyl–$(Glycine)_8$-Glutamine-Tryptophan-Alanine-Valine-Glycine-Histidine-Leucine-Methionine-NH_2 ($(Gly)_8$–Gln–Trp–Ala–Val–Gly–His–Leu–Met–NH_2) (>95% purity by HPLC) was obtained from TAG Copenhagen (Frederiksberg, Denmark). *S*-2-(4-isothiocyanatobenzyl)-1,4,7,10-tetraazacyclododecane tetraacetic acid (p-SCN-Bn-DOTA) was purchased from Macrocyclics (Plano, TX, USA). Ready-to-use hydrazinonicotinamide (HYNIC)–BN kit for the preparation of pentetate (Sn) ^{99m}Tc–BN (Pars-TCK-2600) and ^{68}Ge/^{68}Ga generator (20 mCi/elution activity, radionuclide

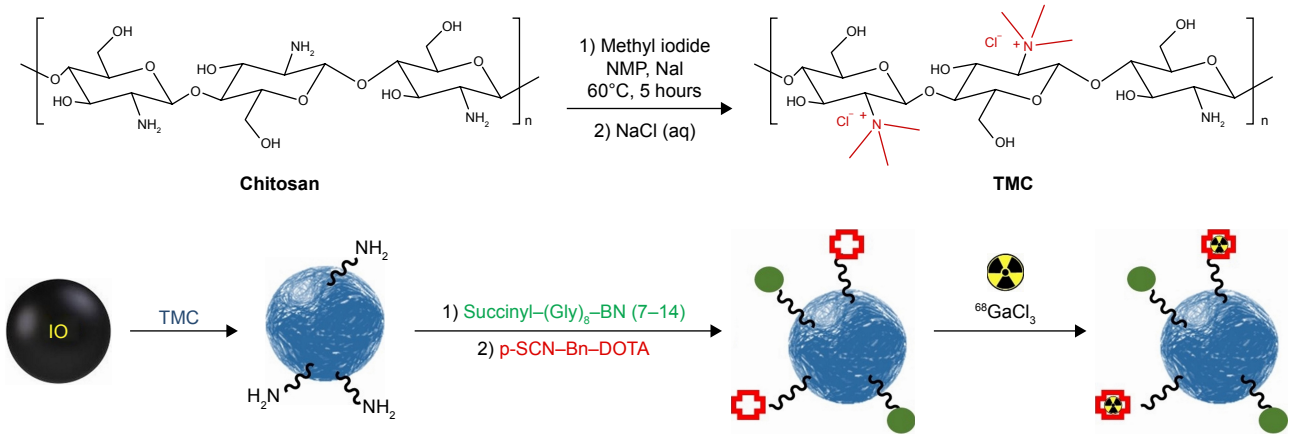

Figure 1 Schematic illustration of the synthesis and radiolabeling of DOTA-BN-TMC-MNPs.
Abbreviations: DOTA, *S*-2-(4-isothiocyanatobenzyl)-1,4,7,10-tetraazacyclododecane tetraacetic acid; BN, bombesin; TMC, *N,N,N*-trimethyl chitosan; MNP, magnetic nanoparticle; NMP, *N*-methyl-2-pyrrolidone.

purity >99%, radiochemical purity [RCP] >98%, ^{68}Ge breakthrough <0.00007% of total radioactivity) was a gift from Pars Isotope Co. (Tehran, Iran). T-47D cell line was obtained from the Iranian Biological Resource Center (Tehran, Iran). The ^{68}Ge/^{68}Ga generator was eluted by hydrochloric acid solution (0.2 M) and 0.5 mL fractions were collected. The fractions 2–4 were applied for the radiolabeling procedure.

Preparation of NP probes

Synthesis of SPIONs

Magnetic nanoparticles (MNPs) were synthesized using the coprecipitation method.[24] Ammonium hydroxide (25%) was added dropwise to a solution of 0.149 g $FeCl_2 \cdot 4H_2O$ and 0.405 g $FeCl_3 \cdot 6H_2O$ in degassed deionized water under nitrogen atmosphere at 70°C until a final pH of 11 was reached and stirred for additional 1 hour at 70°C. Fe_3O_4 NPs were magnetically decanted and washed several times with deionized water and finally dried in a vacuum oven at 40°C.

Synthesis of TMC

The procedure was carried out according to the reported protocol by Atyabi et al[25] with minor modification. A total of 0.5 g chitosan (110–150 kDa, 95% degree of deacetylation) was dispersed in 20 mL *N*-methyl-2-pyrrolidone (NMP) at 60°C followed by the addition of sodium iodide (1.2 g, 8.0 mmol), sodium hydroxide aqueous solution (2.75 mL, 15% w/v), and methyl iodide (3 mL, 48.2 mmol), and the mixture was stirred for 5 hours at 60°C. The product (TMC iodide) was precipitated with acetone, centrifuged (18,000 rpm, 5 minutes), and washed twice with acetone. The sediment was dissolved in 20.0 mL of sodium chloride aqueous solution (10% w/v) to exchange the iodide ions with chloride ions. The resultant solution was dialyzed against distilled water using a dialysis membrane (molecular weight cutoff 12 kDa; Sigma) for 1 day and finally lyophilized.

Synthesis of TMC-coated MNPs (TMC–MNPs)

Iron oxide NPs (5 mg) were dispersed in deionized water (1 mL) using an ultrasonic probe sonicator (amplitude 50%, 18 W) for 30 minutes followed by the addition of TMC dissolved in deionized water (0.125 mL, 50 mg/mL) and shaken for 24 hours at room temperature. The mixture was then centrifuged (25,000 rpm, 20 minutes), and the product was washed using deionized water (2×).

Synthesis of succinyl–$(Gly)_8$–BN (7–14)–TMC–MNP conjugates (BN–TMC–MNPs)

The conjugation was performed by carboxyl-to-amine cross-linking using ethyl-3-[3-(dimethylamino)propyl]carbodiimide (EDC)/*N*-hydroxysuccinimide (NHS) coupling method.[26] Aqueous solutions of EDC (1 mg/mL, 0.2 mL), NHS (1 mg/mL, 0.1 mL), and succinyl–$(Gly)_8$–BN (7–14) (10 mg/mL, 40 µL) were added to a mixture of TMC–MNPs (5 mg) and agitated for 24 hours at room temperature. The product (BN–TMC–MNPs) was purified by centrifuging the reaction mixture (25,000 rpm, 20 min) and washing with deionized water (2×).

Synthesis of DOTA–BN–TMC–MNPs

The synthesis was performed using amine groups of TMC on the surface of NPs according to the reported procedure.[27] To a mixture of BN–TMC–MNPs (5 mg) in carbonate buffer (0.1 M, pH 8.5), *p*-SCN–Bn–DOTA (0.9 mg, 1.31 µmol) was added. DOTA-conjugated BN–TMC–MNPs

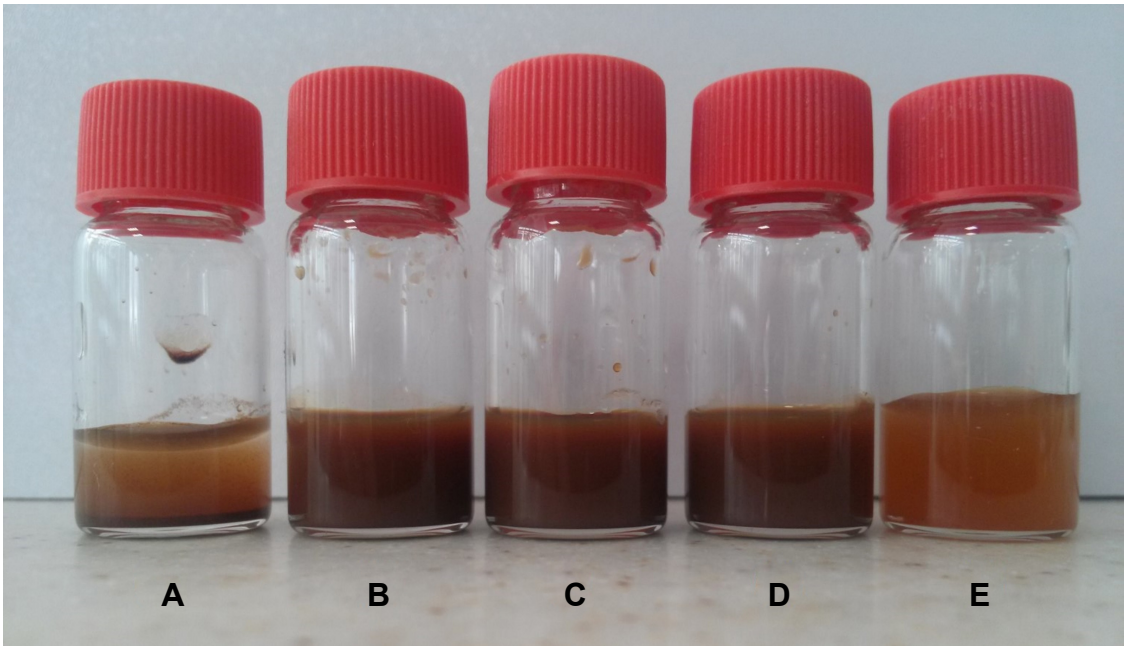

Figure 2 Photographs of (**A**) MNPs, (**B**) TMC–MNPs, (**C**) BN–TMC–MNPs, (**D**) DOTA–BN–TMC–MNPs, and (**E**) ^{68}Ga–DOTA–BN–TMC–MNPs in suspension. TMC–MNPs, BN–TMC–MNPs, DOTA–BN–TMC–MNPs, and ^{68}Ga–DOTA–BN–TMC–MNPs showed dispersion stability in suspension, but MNPs (**A**) precipitated quickly.
Abbreviations: MNP, magnetic nanoparticle; TMC, *N*,*N*,*N*-trimethyl chitosan; BN, bombesin; DOTA, *S*-2-(4-isothiocyanatobenzyl)-1,4,7,10-tetraazacyclododecane tetraacetic acid; ^{68}Ga, gallium-68.

(DOTA–BN–TMC–MNPs) were precipitated by centrifugation (30,000 rpm, 30 minutes) and washed with water. Figure 2 shows the MNPs, TMC–MNPs, BN–TMC–MNPs, and DOTA–BN–TMC–MNPs in the suspension form.

Characterization of NPs

The crystalline properties of MNPs and TMC–MNPs were characterized by powder X-ray diffraction (PXRD; PW1800; Philips) with 2θ range of 20–80 and wavelength of Cu·Kα radiation (1.5409 Å). Hydrodynamic diameter, size distribution, and zeta potential of all synthesized NPs were measured by dynamic light scattering (DLS) instrument with the detection angle of 90° at the wavelength of 633 nm at 25°C (Nano-ZS; Malvern Instruments, Malvern, UK). Transmission electron microscopy (TEM) (CEM 902A; Zeiss, Oberkochen, Germany) was applied to observe the morphology of MNPs, TMC–MNPs, BN–TMC–MNPs, and DOTA–BN–TMC–MNPs. Chemical structure of all-prepared NPs and TMC polymer were evaluated by Fourier transform infrared (FTIR) spectroscopy (Spectrum two, PerkinElmer, USA). Magnetic properties of MNPs and TMC–MNPs were determined using vibration sample magnetometer (VSM) at room temperature (Model 155; Princeton Applied Research, Oak Ridge, TN, USA).

The degrees of quaternization (DQ) and dimethylation (DD) of TMC were calculated using ^{1}H-nuclear magnetic resonance (^{1}HNMR) spectrum (Avanace 500 MHz; Bruker, Rheinstetten, Germany), obtained in D_2O as a solvent,[28,29] and primary amine groups of TMC were measured by the ninhydrin method.[30] The reaction of chitosan, TMC, and glucosamine as a standard compound with the ninhydrin reagent was carried out at 100°C for 16 minutes, and then, the absorption of solutions was read at 570 nm using UV–VIS spectroscopy (CE7500; Cecil, Cambridge, UK). A linear calibration curve was drawn using glucosamine absorptions, and the percentage of free amine groups in TMC was calculated via the absorption of TMC and chitosan.

Thermogravimetric analysis (TGA) of MNPs and TMC–MNPs was used to measure the mass of TMC coated on MNPs surfaces. Because of the presence of sulfur atom in the peptide structure, conjugation of BN to TMC–MNPs was confirmed using elemental analysis (Costech Elemental Combustion System CHNS–O, ECS 4010).

Determination of ferric ion concentration

Colorimetric analyses are commonly applied for the evaluation of iron content in chemical and biological samples. Ferric ions (Fe^{3+}) can form brick-red ferric thiocyanate complexes after reacting with thiocyanate ions (SCN^{-}), which show a good linearity at a broad range of Fe^{3+}concentrations.

Aliquots (10 µL) of DOTA–BN–TMC–MNPs in deionized water and standard solutions of iron (III) nitrate

nonahydrate ($Fe(NO_3)_3 \cdot 9H_2O$) were added into an equal volume of 12% HCl and agitated for 30 minutes. Aliquots of the obtained solutions (50 µL) were added into a 96-well plate followed by the addition of 1% ammonium persulfate solution (50 µL) into each well. Brick-red ferric thiocyanate complexes formed by the addition of potassium thiocyanate solution (100 µL, 0.1 M) were assayed using a microplate reader at a wavelength of 490 nm (BioTek ELx800).[31] The ferric ion concentration of DOTA–BN–TMC–MNPs was calculated from the equation of the calibration curve and the absorbance of the sample.

Phantom study

To measure the relaxation characteristics of the DOTA–BN–TMC–MNPs as a T_2-weighted MRI contrast media, varying concentrations of DOTA–BN–TMC–MNPs ranging from 25 to 200 µM for Fe in deionized water containing 1% agarose were filled into 2.0 mL microcentrifuged tubes. The T_2-weighted images were acquired using a 3T MRI Scanner (Magnetom Prisma) with a repetition time (T_R) of 2,500 milliseconds, echo time (T_E) of 14.2–142 milliseconds, flip angle of 180°, and matrix measuring 384×252.

Radiolabeling of NPs

An aliquot of DOTA–BN–TMC–MNPs (100 µL, 5 mg/mL) dispersed in acetate buffer (100 mM, pH 4.9) was added to 700 µL (148 MBq) of $^{68}GaCl_3$ solution eluted by 0.2 M HCl containing 100 mg HEPES in a 10 mL borosilicate vial. The mixture was vortexed for 10 s and heated at 90°C for 5 min. RCP was evaluated by instant thin layer chromatography-silica gel (ITLC-SG) using sodium citrate solution (100 mM) as mobile phase and radiochromatograms were plotted by a TLC scanner (MiniGita, Elysia-Raytest, Germany).

Stability test in human serum

The stability of ^{68}Ga-radiolabeled DOTA–BN–TMC–MNPs in human serum was assessed by ITLC-SG and sodium citrate solution (100 mM) as the mobile phase.[32] Radiolabeled NPs were incubated in human serum (1:10 ratio) at 37°C for 180 minutes, and RCP was determined every 30 minutes by TLC. All assays were done in triplicate.

In vitro assays

Cell culture

GRP receptor-expressing human BC cell line T-47D was cultured in DMEM (high glucose; Biosera, Nuaillé, France) supplemented with 10% FBS and 1% penicillin–streptomycin in a humidified atmosphere at 37°C with 5% CO_2.

Cytotoxicity assay

The cytotoxicity of DOTA–BN–TMC–MNPs was investigated by MTT assay. The T-47D cells were seeded in 96-well plates (5,000 cells/well) and incubated for 24 hours. Cells were treated at the NPs' concentration range of 0.1–200 µg/mL in PBS and incubated at 37°C with 5% CO_2 for 24 and 48 hours. After each interval, the cells' medium was replaced with 50 µL of MTT reagent (0.5 mg/mL in PBS) and incubated for 3 hours at 37°C and 5% CO_2. Afterward, 150 µL of DMSO was added to each well to dissolve formazan crystals, and the absorbance was read at 570 nm with a reference wavelength of 630 nm using a microplate reader.

In vitro competitive cell-binding assay

Competitive cell-binding assay was used to evaluate the IC_{50} value of DOTA–BN–TMC–MNPs in GRP receptor-expressing human BC cell line T-47D.[33] The IC_{50} value was determined against ^{99m}Tc–HYNIC–gamma-aminobutyric acid (GABA)–BN (7–14) as a standard GRP receptor binding agent.[34] In order to measure the IC_{50} value, the total concentration of receptors expressed on T-47D cells (B_{max}) was determined using the saturation binding assay.

The HYNIC–GABA–BN (7–14) cold kit was labeled with $^{99m}TcO_4^-$ solution (20 mCi, 1,200 Ci/mmol) according to the kit labeling instruction. In all, 400 µL of T-47D cells (1×10^5 cells) in PBS were incubated with 100 µL of ^{99m}Tc–HYNIC–GABA–BN (7–14) (5–300 nM in PBS) in triplicate for 1 hour at 37°C. Nonspecific binding (NSB) of radiolabeled peptide was estimated using the incubation of excess unlabeled peptide (10 µM) to block the specific binding sites for 30 minutes at 37°C. At the end of the incubation times, cells were centrifuged (1,200 rpm, 5 minutes), the cell pellets were washed with cold PBS, and their radioactivity was measured using an NaI well counter (Triathler Multilabel Tester; Hidex, Turku, Finland).

In order to evaluate the IC_{50} value of DOTA–BN–TMC–MNPs, T-47D cells were aliquoted into 2 mL microcentrifuged tubes (1×10^5 cells), and the ^{99m}Tc–HYNIC–GABA–BN (7–14) (100 µL, 240 nM) cells were added, followed by the addition of various concentrations of DOTA–BN–TMC–MNPs (0.001–60 µg/mL, 46.8 pM–2.81 µM BN) in triplicate. The tubes were shaken at 4°C for 1 hour, and after the incubation time, cells were centrifuged for 5 minutes and washed with cold PBS. The radioactivity of cell pellets was measured using a gamma counter. The IC_{50} value of DOTA–BN–TMC–MNPs

was obtained by plotting the radioactivity of ^{99m}Tc-HYNIC–GABA–BN (7–14) versus the log of the DOTA–BN–TMC–MNPs concentrations using GraphPad Prism Software (GraphPad Software, Inc., La Jolla, CA, USA).

In vivo assays

Animal model development

All animal experiments were performed in accordance with National Research Council's Guide for the Care and Use of Laboratory Animal's ethical guidelines/regulations, and the investigation was approved by the ethical committee of Tehran University of Medical Sciences (Code no 1394.223). In all, 8-week-old female athymic nude mice (Pasteur Institute of Iran) were subcutaneously implanted with 3×10^6 T-47D cells in 0.1 mL PBS into the right leg or shoulder. A total of 10–12 days after cell implantation, MRI or PET and biodistribution study in tumor-bearing nude mice were investigated. Normal biodistribution of ^{68}Ga–DOTA–BN–TMC–MNPs was studied in 8-week-old female Balb/C mice.

Biodistribution studies

Solutions of ^{68}Ga–DOTA–BN–TMC–MNPs (3.7 MBq) were injected to the normal Balb/C and tumor-bearing nude mice through the tail vein. The percentage of radioactivity in different organs was calculated at 30, 60, 90, and 120 minutes post-injection.

In vivo imaging studies

For animal MRI, shoulder xenograft nude mice were used. The tumor-bearing nude mice were anesthetized by ketamine/xylazine, and magnetic resonance (MR) images were obtained pre and post-injection of 100 µL DOTA–BN–TMC–MNPs (1 mg/mL, 5.12 mM Fe) in deionized water. The T_2-weighted fast spin-echo imaging was performed using a 3T MRI under the following conditions: T_R/T_E: 2,300/110 milliseconds, flip angle: 150°, echo train length: 15, slice thickness: 2 mm, and matrix: 256×216.

PET/CT imaging of T-47D tumor-bearing nude mice in the right leg was accomplished using Siemens Biograph TruePoint PET/CT scanner (Siemens AG, Erlangen, Germany). The CT scans of the mice in the supine position were performed for anatomical reference and attenuation correction (spatial resolution 1.25 mm, 80 kV, 30 mAs). Static PET acquisitions were performed with three sets of emission images after injection of 3.7 MBq ^{68}Ga–DOTA–BN–TMC–MNPs starting at 30, 60, and 120 minutes. Attenuated corrected PET images were reconstructed using the ordered subsets expectation-maximization (OSEM) algorithm with four iterations and 21 subsets into a 256×256 matrix smoothed using a Gaussian kernel of 3 mm full width at half maximum (FWHM). Transmission data were reconstructed into a matrix of equal size by means of filtered back projection, yielding a co-registered image set. The reconstructed PET images were then fused with CT images.

Results

Characterization of synthesized NPs

The crystalline structure of Fe_3O_4 NPs and TMC–MNPs assayed by PXRD is shown in Figure 3A. Six significant peaks for MNPs at 2θ=30.2, 35.6, 43.2, 53.7, 57.1, and 62.9 were observed in both Fe_3O_4 NP and TMC–MNPs patterns.[35]

Magnetic properties of Fe_3O_4 NPs and TMC–MNPs were evaluated using the VSM method (Figure 3B), and the saturation magnetization values for MNPs and TMC–MNPs were obtained as 96.5 and 52 emu/g, respectively. The saturation magnetization of TMC-coated MNPs was lost after the coating process, nevertheless both MNPs and TMC-coated MNPs present superparamagnetic behavior because the coercivity (H_c) of both curves was found to be zero.

The mass of TMC coated on MNPs surfaces was measured by TGA. TGA curves of pure Fe_3O_4 NPs and TMC–MNPs (Figure 3C) show 1.93% and 1.67% weight loss in the temperature range of about 25°C–150°C, which relates to the loss of residual water in the samples. Weight loss between 150 and 400°C in the TGA curve of TMC–MNPs (6.72%) demonstrates weight percentage of polymer coated on MNP surfaces.

Hydrodynamic diameter, size distribution, and zeta potential of all synthesized NPs measured by DLS have been given in Table 1.

Presence and content of BN peptides on TMC–MNPs were evaluated by CHNS elemental analysis of TMC–MNPs and BN–TMC–MNPs using the measurement of sulfur atoms in methionine amino acids. Based on the obtained weight percent of sulfur in samples, the peptide content was calculated as 0.07 mg per 1 mg of BN–TMC–MNPs.

Primary amine groups of TMC were measured by the ninhydrin method using glucosamine as a standard compound.[30] Compared to chitosan, 33.7% of primary amine groups were present in the TMC structure after the methylation process.

^{1}HNMR spectrum was applied to confirm the introduction of methyl groups at the primary amine groups of chitosan and calculate the DQ and DD in the TMC structure. ^{1}HNMR spectrum of TMC chloride and chitosan showed the signals at 2.85 and 3.06 ppm attributed to the $N(CH_3)_2$ and $N(CH_3)_3$ groups, respectively. The signals at 2.04, 3.78–4.57, and 5.11–5.43 ppm were assigned to the methyl protons of the acetamide groups, H2–H6, and H1 protons in the chitosan

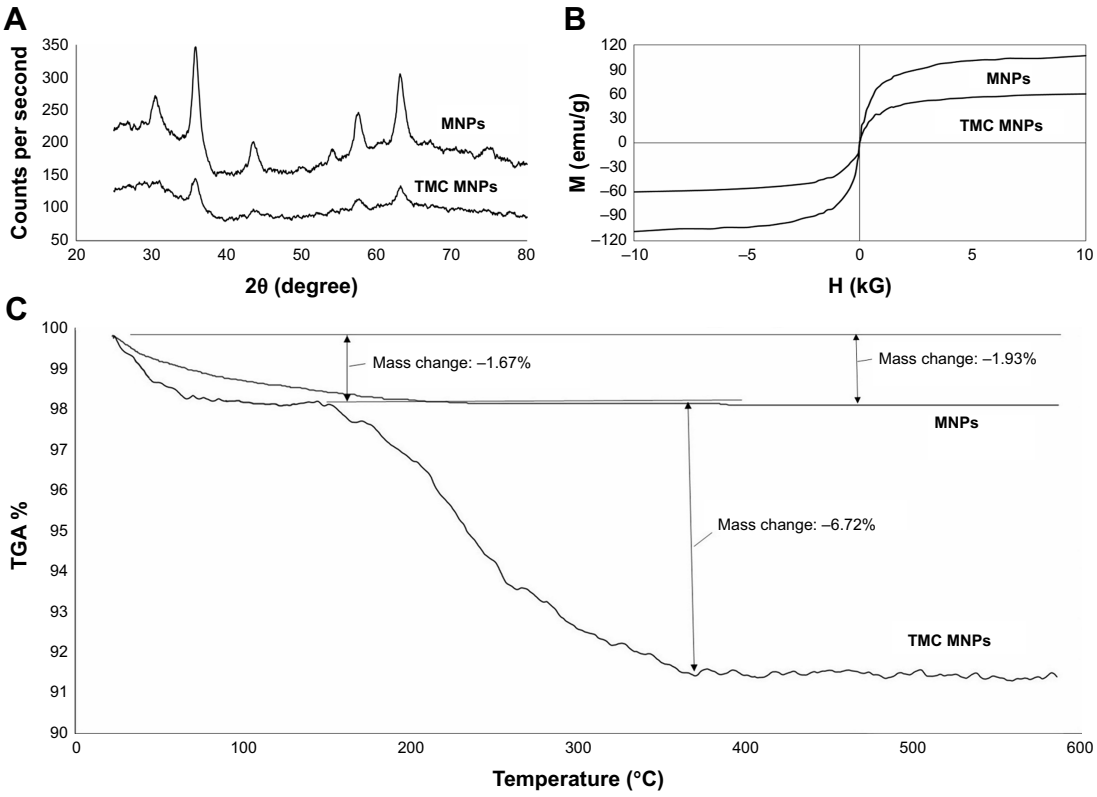

Figure 3 Characterization of MNPs and TMC–MNPs using PXRD, VSM, and TGA. (**A**) PXRD patterns of MNPs and TMC–MNPs. (**B**) TGA curves of MNPs and TMC–MNPs. (**C**) Hysteresis curves of MNPs and TMC–MNPs.
Abbreviations: H, magnetic field; M, magnetization; MNP, magnetic nanoparticle; TMC, *N,N,N*-trimethyl chitosan; PXRD, Powder X-ray diffraction; VSM, vibrating sample magnetometer; TGA, thermogravimetric analysis.

structure, respectively. The signal at 3.33 ppm in chitosan and TMC ^{1}HNMR spectra can be attributed to the H2 of deacetylated monomers in the chitosan structure and OCH_3 protons in TMC polymers. The DQ and DD were calculated 51.3% and 12.8%, respectively.[28,29,36]

Figure 4 displays FTIR spectra of Fe_3O_4 NPs, TMC, TMC-coated MNPs, BN–TMC–MNPs, and DOTA–BN–TMC–MNPs. The strong absorption at 584 cm^{-1} corresponds to the stretching vibration of Fe–O band of Fe_3O_4 NPs and exists in other spectra except for the TMC spectrum. The O–H stretch is a broad peak at 3,000–3,430 cm^{-1} (Figure 4A). The TMC spectrum showed absorption peaks at 1,634 cm^{-1} (C=O stretching of amide II), 1,057 cm^{-1} (C–O and C–N stretching), and 3,437 cm^{-1} (O–H and NH stretching) and characteristic bending absorption at 1,368 cm^{-1} for methyl groups (Figure 4B). FTIR spectra of TMC–MNPs in Figure 4C exhibit characteristic bands of TMC and pure MNPs, which demonstrates the polymer coating of MNPs. The BN–TMC–MNPs spectrum (Figure 4D) shows that the peaks at 1,537, 1,634, and 3,282 cm^{-1} are assigned to the N–H bending of amide I and II, C=O band of amide I, and N–H stretch in primary amides in the BN sequence, respectively (Gln side chain and c-terminal amide of BN). In the DOTA–BN–TMC–MNPs spectrum (Figure 4E), the carbonyl groups of DOTA carboxylic acid moieties appeared at 1,734 cm^{-1}, which demonstrates DOTA linking to the NPs.

Figure 5A–D exhibits the TEM images of MNPs, TMC–MNPs, BN–TMC–MNPs, and DOTA–BN–TMC–MNPs in which the <30 nm spherical NPs in all images are distinguished. As seen in Figure 5D, a very thin layer of TMC polymer is visible on the surface of MNPs.

Table 1 Size, PDI, and zeta potential of NPs

NPs	Size (nm)	PDI	Zeta potential (mV)
MNPs	43.2±3.7	0.157	−1.56±0.23
TMC–MNPs	55.1±4.3	0.249	+32.4±3.27
BN–TMC–MNPs	68.7±3.4	0.140	+36.8±4.41
DOTA–BN–TMC–MNPs	69.2±5.1	0.133	+16.8±1.86

Note: Values represent mean±SD, n=3.
Abbreviations: PDI, polydispersity index; NPs, nanoparticle; MNP, magnetic nanoparticle; TMC, *N,N,N*-trimethyl chitosan; BN, bombesin; DOTA, *S*-2-(4-isothiocyanatobenzyl)-1,4,7,10-tetraazacyclododecane tetraacetic acid.

Radiolabeling of NPs

In thin layer chromatography studies, free ^{68}Ga (III) cations form ^{68}Ga citrate complexes and migrate to R_f 0.6, while

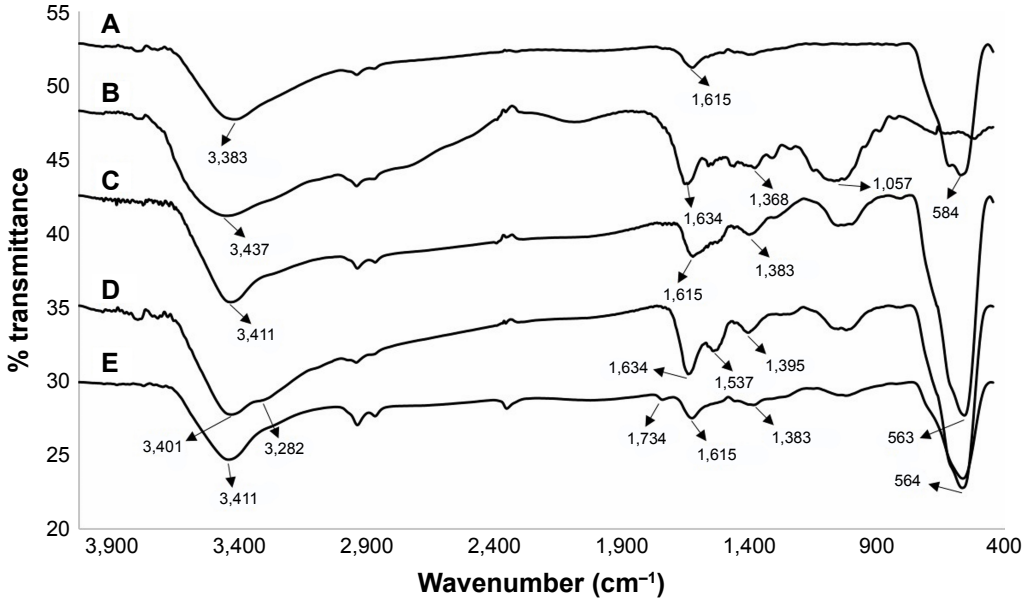

Figure 4 FTIR spectra of (**A**) MNPs, (**B**) TMC, (**C**) TMC–MNPs, (**D**) BN–TMC–MNPs, and (**E**) DOTA–BN–TMC–MNPs.
Abbreviations: FTIR, Fourier transform infrared; MNP, magnetic nanoparticle; TMC, *N*,*N*,*N*-trimethyl chitosan; BN, bombesin; DOTA, *S*-2-(4-isothiocyanatobenzyl)-1,4,7,10-tetraazacyclododecane tetraacetic acid.

the radiolabeled NPs retain at the base (R_f 0.1). ^{68}Ga–DOTA–BN–TMC–MNPs' RCP was higher than 98% (46,250 MBq/mmol Fe), which could be used without further purification for later studies.

Stability in human serum

^{68}Ga-radiolabeled DOTA–BN–TMC–MNPs were incubated in human serum at 37°C for 180 minutes, and RCP was checked every 30 minutes by radio-TLC as mentioned in

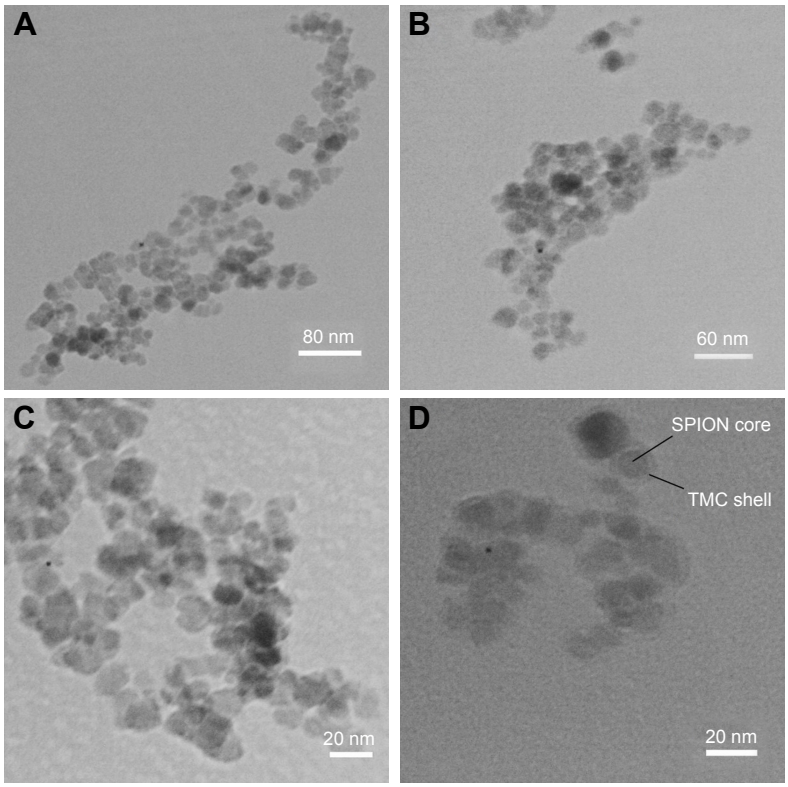

Figure 5 TEM images of (**A**) MNPs, (**B**) TMC–MNPs, (**C**) BN–TMC–MNPs, and (**D**) DOTA–BN–TMC–MNPs.
Abbreviations: TEM, transmission electron microscopy; MNP, magnetic nanoparticle; TMC, *N*,*N*,*N*-trimethyl chitosan; BN, bombesin; DOTA, *S*-2-(4-isothiocyanatobenzyl)-1,4,7,10-tetraazacyclododecane tetraacetic acid; SPION, superparamagnetic iron oxide nanoparticle.

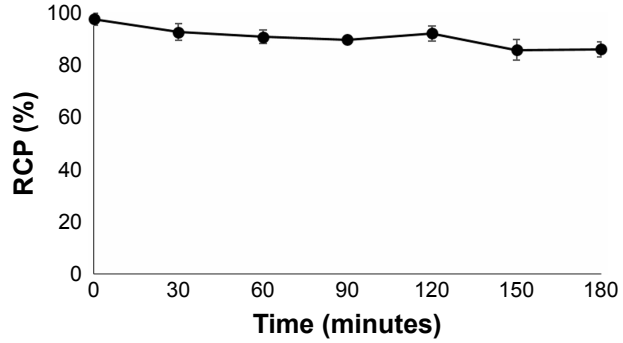

Figure 6 RCP of ^{68}Ga–DOTA–BN–TMC–MNPs in human serum at 37°C. Values represent the mean±SD, n=3.
Abbreviations: RCP, radiochemical purity; ^{68}Ga, gallium-68; DOTA, *S*-2-(4-isothiocyanatobenzyl)-1,4,7,10-tetraazacyclododecane tetraacetic acid; BN, bombesin; TMC, *N*,*N*,*N*-trimethyl chitosan; MNP, magnetic nanoparticle.

the "Materials and methods" section. ^{68}Ga citrate complexes migrate to R_f 0.5–0.7 on ITLC-SG using sodium citrate solution as the mobile phase, while the ^{68}Ga-labeled NPs retain at the base (R_f 0.1). As shown in Figure 6, ^{68}Ga–DOTA–BN–TMC–MNPs had 92% stability after 120 minutes and 86% stability after 180 minutes.

Cytotoxicity assay

In vitro cytotoxicity of DOTA–BN–TMC–MNPs on T-47D cells at the concentration range of 0.1–200 µg/mL showed insignificant toxicity for the cells in comparison with that for the nontreated cells (Figure 7), and 76.7%±2.9% and 74.0%±3.7% of the cells were survived in contact with the highest concentration (200 µg/mL) of NPs after 24 and 48 hours.

In vitro competitive cell-binding assay

The total concentration of GRP receptors expressed on T-47D cells (B_{max}) and dissociation constant (K_d) for ^{99m}Tc–HYNIC–GABA–BN (7–14) were determined using saturation binding assay. As depicted in Figure 8A, specific binding

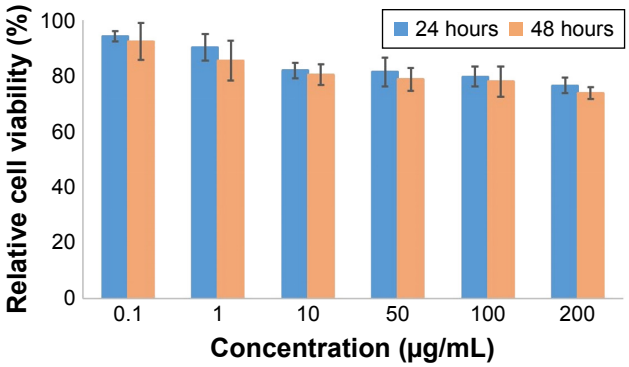

Figure 7 MTT assay of DOTA–BN–TMC–MNPs on T-47D cells after 24 and 48 hours.
Abbreviations: DOTA, *S*-2-(4-isothiocyanatobenzyl)-1,4,7,10-tetraazacyclododecane tetraacetic acid; BN, bombesin; TMC, *N*,*N*,*N*-trimethyl chitosan; MNP, magnetic nanoparticle.

of ^{99m}Tc–HYNIC–GABA–BN (7–14) to GRP receptors on the cell surfaces was plotted versus the concentration of the radiopeptide added. The B_{max} and K_d values were calculated using GraphPad Prism 7 Software (nonlinear regression analysis, binding saturation, one site-specific binding) as 212.1 and 17.86 nM, respectively.

The IC_{50} value of DOTA–BN–TMC–MNPs was evaluated using the competitive binding assay against ^{99m}Tc–HYNIC–GABA–BN (7–14) in BC T-47D cells (Figure 8B). The IC_{50} value of DOTA–BN–TMC–MNPs was 8.79 µg/mL (411.1 nM for BN).

Biodistribution studies

The percentage of injected dose per gram of organs (%ID/g) for ^{68}Ga–DOTA–BN–TMC–MNPs in normal Balb/C and tumor-bearing mice was determined at 30, 60, 90, and 120 minutes post-injection (Figure 9A). Radiolabeled NPs were rapidly cleared from the circulation by the reticuloendothelial system (RES) cells in the liver and spleen. Compared to the normal model, the percentage of ID/g for all organs significantly did not change in tumor-bearing mice. The percent tumor uptake of radiolabeled NPs was 0.78% at 30 minutes, 1.56% at 60 minutes, 1.75% at 90 minutes, and 2.27% at 120 minutes, which indicated incremental accumulation of targeted NPs in the tumor. As shown in Figure 9B, tumor-to-tissue ratios also confirmed increasing uptake of NPs in the tumor over the time.

MRI studies

Relaxation characteristics of DOTA–BN–TMC–MNPs were measured using serially diluted aqueous solutions of 200 µM DOTA–BN–TMC–MNPs for Fe. T_2-weighted images of solutions (Figure 10A) showed decreased signal intensity when the Fe concentration rose, and the T_2 relaxivity (r_2) was calculated as 330.98 $mM^{-1}\cdot s^{-1}$ for DOTA–BN–TMC–MNPs (Figure 10B).

MRI of T-47D tumor-bearing mice at shoulder has been shown in Figure 10C before and Figure 10D after administration of DOTA–BN–TMC–MNPs. The decrease in MR signals in tumor lesion due to the specific uptake of DOTA–BN–TMC–MNPs made this region darker (yellow circle in Figure 10D) and improved the image contrast as a result.

PET imaging studies

PET/CT images were acquired at 30, 60, and 120 minutes post-injection of 3.7 MBq ^{68}Ga–DOTA–BN–TMC–MNPs in T-47D tumor-bearing mice. As shown in Figure 10E, there is the most activity concentration in liver and tumor. The activity in the spleen and bladder is slightly higher than the

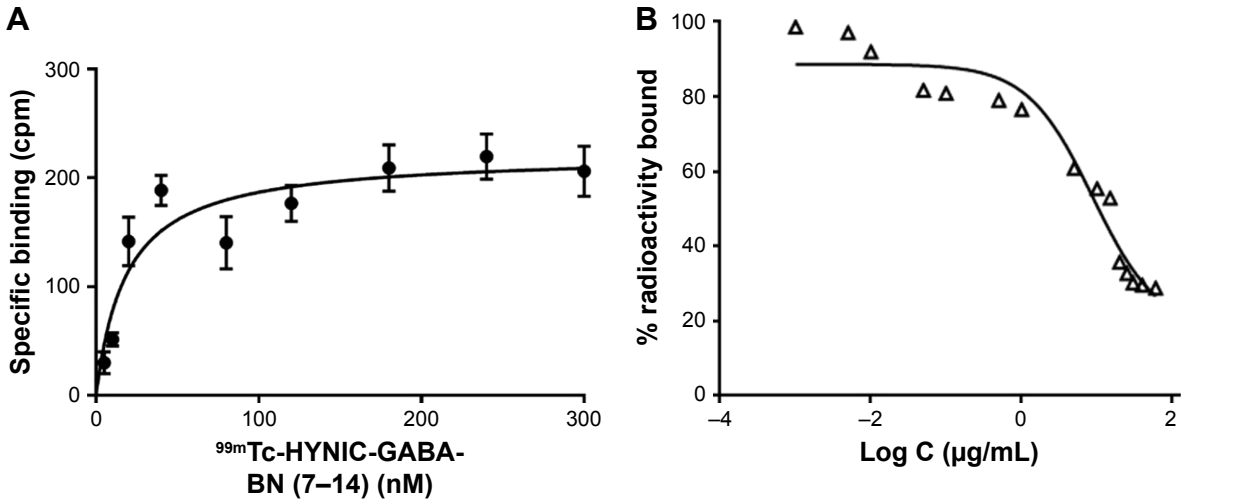

Figure 8 (**A**) Saturation binding study of ^{99m}Tc–HYNIC–GABA–BN (7–14) to GRP receptors of T-47D cells and (**B**) inhibition of ^{99m}Tc–HYNIC–GABA–BN (7–14) binding to T-47D cells with the various concentrations of DOTA–BN–TMC–MNPs. Results of a representative experiment are expressed as the percentage of radioactivity bound to the cells (mean±SD, n=3).

Abbreviations: ^{99m}Tc, Technetium-99m; HYNIC, hydrazinonicotinamide; GABA, gamma-aminobutyric acid; BN, bombesin; GRP, gastrin-releasing peptide; DOTA, *S*-2-(4-isothiocyanatobenzyl)-1,4,7,10-tetraazacyclododecane tetraacetic acid; TMC, *N*,*N*,*N*-trimethyl chitosan; MNP, magnetic nanoparticle.

background activity 120 min post-injection. Quantitative assessment of PET/CT images was performed by measurement of maximum and peak standardized uptake values, SUV_{max} and SUV_{peak}, for tumor inoculated in the right leg, left leg (control), and liver.

Discussion

At present, the development of MRI contrast agents radiolabeled with positron emitters as PET/MR dual-modality imaging probes is an attractive field of research. PET/MRI can merge the high spatial resolution of MRI with an excellent sensitivity and quantitative data analysis of PET.[17] Compared to the gadolinium chelates, higher biocompatibility and modifiable SPIONs surfaces offer targeted and radiolabeled SPIONs as T_2-weighted PET/MR dual imaging probes for early detection of cancers.[37]

The high mortality rate of BC in women has led to the crucial need for early and accurate diagnosis of malignant lesions.

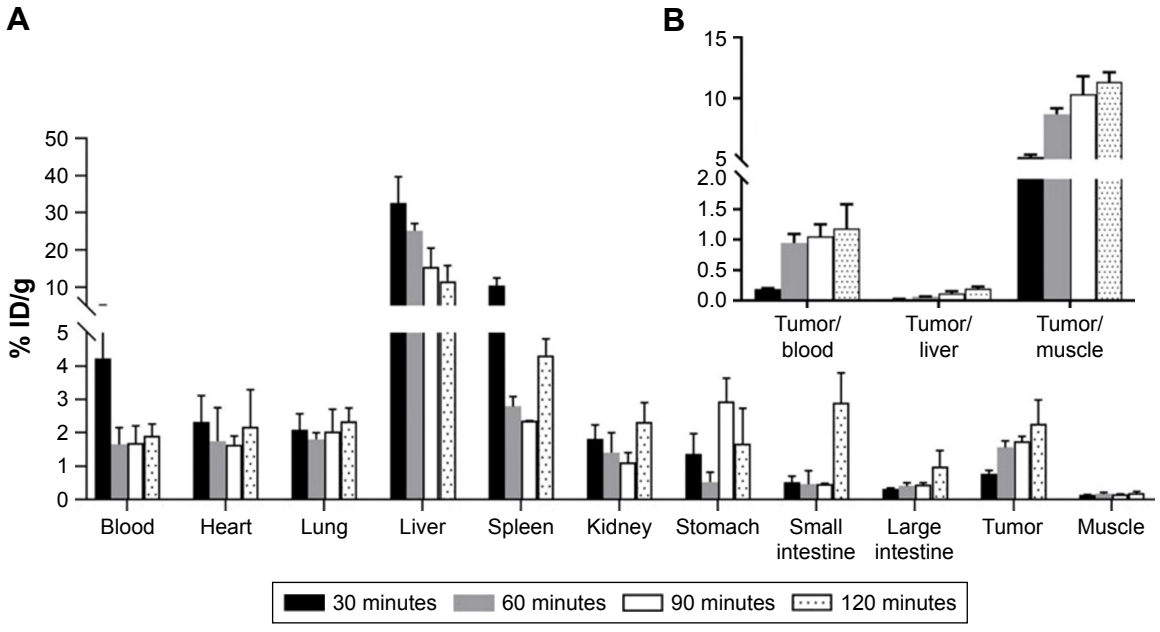

Figure 9 (**A**) Biodistribution of ^{68}Ga–DOTA–BN–TMC–MNPs in tumor-bearing mice at 30, 60, 90, and 120 minutes post-injection (ID%/g±SD, n=3) and (**B**) tumor-to-organ ratios at 30, 60, 90, and 120 minutes post-injection.

Abbreviations: %ID/g, percent injected dose per gram; ^{68}Ga, gallium-68; DOTA, *S*-2-(4-isothiocyanatobenzyl)-1,4,7,10-tetraazacyclododecane tetraacetic acid; BN, bombesin; TMC, *N*,*N*,*N*-trimethyl chitosan; MNP, magnetic nanoparticle.

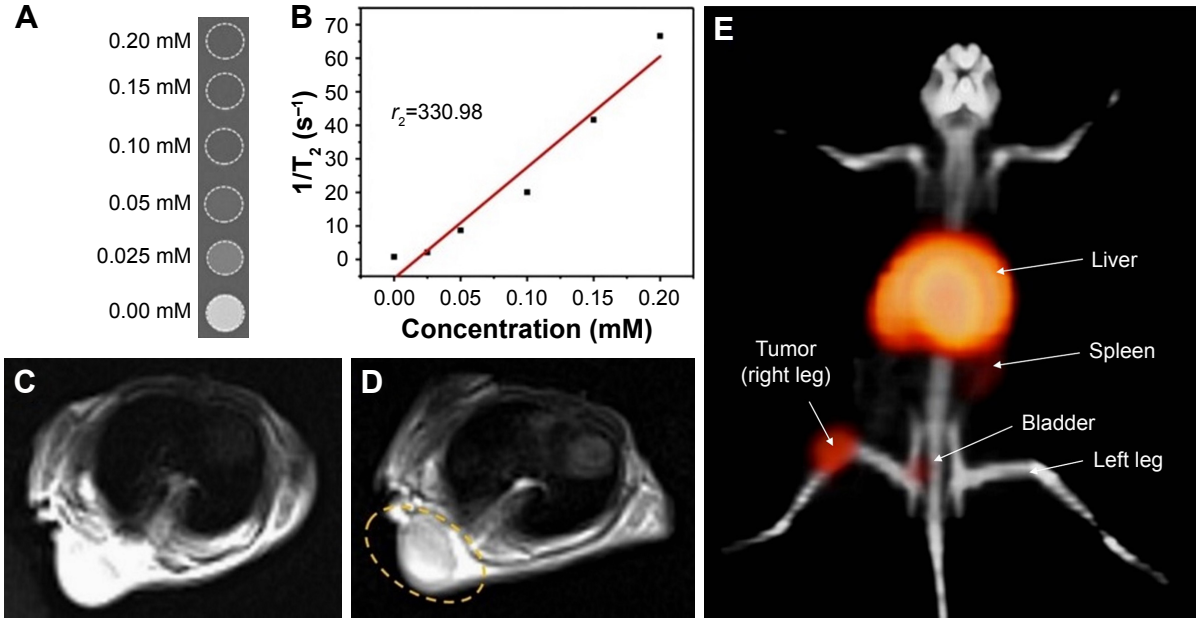

Figure 10 Phantom study, MRI, and PET/CT of DOTA–BN–TMC–MNPs and ^{68}Ga–DOTA–BN–TMC–MNPs. (**A**) MRI phantom study of serially diluted aqueous solutions of 200 μM DOTA–BN–TMC–MNPs for Fe and (**B**) relaxation rate ($1/T_2$) as a function of iron concentration. MR images of shoulder xenograft nude mouse (**C**) before and (**D**) after DOTA–BN–TMC–MNPs injection through the tail vein (1 hour) under the 3T magnetic field. Yellow circle demonstrates the uptake of NPs to the tumor. (**E**) PET/CT image of a nude mice bearing T-47D BC tumor in the right leg in the supine position following the injection of 3.7 MBq ^{68}Ga–DOTA–BN–TMC–MNPs after 120 minutes.
Abbreviations: $1/T_2$, relaxation rate; MR, magnetic resonance; MRI, MR imaging; PET, positron emission tomography; CT, computed tomography; DOTA, *S*-2-(4-isothiocyanatobenzyl)-1,4,7,10-tetraazacyclododecane tetraacetic acid; BN, bombesin; TMC, *N*,*N*,*N*-trimethyl chitosan; MNP, magnetic nanoparticle; ^{68}Ga, gallium-68; NP, nanoparticle; BC, breast cancer.

GRP receptors overexpressed on the surface of BC cells can be targeted using BN as a specific ligand attached to the NPs.

In this study, we developed SPIONs coated by TMC and conjugated to BN as targeting ligands and DOTA as ^{68}Ga chelators. Obtained NPs were radiolabeled with ^{68}Ga to detect BC in mice models using MRI and PET techniques.

Uncoated SPIONs tend to agglomerate into larger particles and lose their superparamagnetic properties in suspension.[38] TMC as a water-soluble and cationic derivative of chitosan was selected for coating of SPIONs. Designed NPs containing SPIONs covered with TMC showed a good stability in aqueous media in a broad range of pHs required for DOTA–BN–TMC–MNPs synthesis and radiolabeling procedures.

Since the primary amine groups of TMC were needed for conjugation of Succinyl–$(Gly)_8$–BN (7–14) and *p*-SCN–Bn–DOTA to TMC–MNPs, measurement of primary amine groups in TMC was essential. This estimation was performed by quantitative ninhydrin assay and ^{1}HNMR spectroscopy. Interestingly, ninhydrin assay results were correlated with quantitative measurements of ^{1}HNMR spectrum. TMC was coated on SPIONs by electrostatic interactions between positively charged TMC and anionic MNPs. Furthermore, the chemical affinity of hydroxyl and amine groups in the TMC structure to SPIONs can improve the attachment and stability of coating layer on iron oxide NPs.[39]

Excellent magnetic properties are the mainstay for SPIONs applied as T_2-weighted MRI contrast agents. Magnetic properties of bare SPIONs were as great as the coating process could not dramatically diminish their saturation magnetization based on VSM results.

The evaluation of hydrodynamic diameter revealed that the size of SPIONs was increased following polymer coating and peptide conjugation. However, conjugating of DOTA to BN–TMC–MNPs caused no meaningful change in the hydrodynamic size of NPs due to the small molecular size of p-SCN–Bn–DOTA. Cationic nature of TMC polymer increased significantly the surface charge of MNPs from –1.56±0.23 mV to +32.4±3.27 mV ($P<0.05$). The theoretically calculated charge of the intact peptide (Succinyl–$(Gly)_8$–BN [7–14]) was positive, so peptide conjugation to the surface of TMC–MNPs slightly raised the zeta potential of NPs. The presence of negatively charged carboxylate groups in the DOTA structure diminished the zeta potential of prepared DOTA–BN–TMC–MNPs to +16.8±1.86 mV.

TEM images of DOTA–BN–TMC–MNPs exhibited spherical core–shell shapes with a low thickness of TMC around MNPs. Functionalization of TMC–MNPs with BN and DOTA had the negligible effect on size and morphology of final NPs (Figure 5B).

Peptide conjugation efficiency to NPs has been estimated using UV–VIS spectroscopy and Bradford protein assay.[40,41]

As TMC interfered with the BN content assay using these methods, CHNS analysis was applied to measure peptide content of BN–TMC–MNPs. Considering the presence of a sulfur-containing amino acid (methionine) in the peptide sequence and the absence of sulfur atoms in the chemical structure of TMC–MNPs, the peptide mass was calculated by measuring the number of sulfur atoms in the structure of BN–TMC–MNPs in comparison with that of TMC–MNPs.

Regarding previously reported studies, both pre- and postcoated SPIONs with chitosan have demonstrated good biocompatibility in biological media.[42,43] The MTT test of DOTA–BN–TMC–MNPs on T-47D cells indicated that NPs had no remarkable cytotoxicity even at the highest concentration (200 μg/mL). As more than 80% cell viability was observed at 0.1–100 μg/mL of NPs after 48 hours, this concentration range was chosen for further in vitro assays.

Despite lower stability constant of DOTA ($\log K_{Gal}$=21.3) for ^{68}Ga labeling in comparison with NOTA ($\log K_{Gal}$=31.0)[44,45] and elevated temperature requirement for radiolabeling with ^{68}Ga, DOTA is the preferred macrocyclic chelator to coordinate ^{68}Ga because of the availability of different bifunctional derivatives and sufficient in vivo stability of its complex with Ga(III).[42] Furthermore, DOTA can form stable complexes with such therapeutic radionuclides as yttrium-90 and lutetium-177 to complete a theranostic feature in tandem with ^{68}Ga–DOTA–BN–TMC–MNPs. The stability results of radiolabeled NPs exhibited <7% release of ^{68}Ga from prepared in human plasma and trivial release in labeling mixture during 2 hours.

In vitro competitive binding assay has been performed on T-47D cells using different BN peptide sequences conjugated to the various linkers, chelating agents, and fluorescent dyes against ^{125}I–Tyr^4–BN to determine their binding affinity for GRP receptors. The IC_{50} values of these peptides have been reported between 1.7 and 383 nM.[46,47] There are limited studies on the binding affinity of BN conjugated to NPs for GRP receptors in BC cell lines. Nripen et al[33] have evaluated the cell-binding affinity of gold nanorod–bombesin (GNR–BN) conjugates toward prostate cancer (PC3) and BC (T-47D) cell lines using ^{125}I–Tyr^4–BN as a GRP receptor-specific peptide. The IC_{50} values for GNR–BN conjugates with incremental BN content were reported as 7.57, 3.52, and 2.12 μg/mL in T-47D cells. In this study, the IC_{50} value for DOTA–BN–TMC–MNPs was calculated for T-47D cells using ^{99m}Tc–HYNIC–GABA–BN (7–14). The HYNIC–GABA–BN (7–14) kit is routinely applied for localization, staging, and follow-up care after cancer treatment in breast and prostate tumors with positive GRP receptors using the SPECT scan. The amino acid sequence of BN in this kit contains the C-terminal region of BN, which is the active site and has a high binding affinity to GRP receptors.[48,49] The obtained IC_{50} value for DOTA–BN–TMC–MNPs is 8.79 μg/mL (411.1 nM for BN), and it is assumed that DOTA–BN–TMC–MNPs have great ability to compete with radiopeptides toward GRP receptors.

In vivo validation tests of radiolabeled and cold DOTA–BN–TMC–MNPs were carried out using biodistribution assay, PET/CT, and MRI. Based on biodistribution assessment in normal mice, liver and spleen retained high activity. Notably, the majority of ^{68}Ga–DOTA–BN–TMC–MNPs cleared from blood circulation during the first 30 minutes via Kupffer cells' phagocytic sequestration in the liver. A high liver uptake of NPs has occurred after opsonization of them upon contact with blood and recognition of opsonized proteins by macrophages.[50] Moreover, the activity of small intestine started to increase following the reduction in liver activity, which represents the elimination pathway of NPs. Since the large particles mostly accumulate in the lung, very low detected radioactivity in lung indicates the appropriate size distribution of radiolabeled NPs in serum.

Various factors can influence on the efficient delivery of NPs to malignant tissue in mice models including hydrodynamic diameter, shape, surface charge, and composition of NPs as well as tumor model, cancer type, and targeting strategies. Wilhelm et al[51] after literature survey reported that only 0.7% (median) of the injected dose of NPs is found to reach a solid tumor. Tumor uptake of ^{68}Ga–DOTA–BN–TMC–MNPs was quantified by biodistribution analysis in the tumor mice models. Radiolabeled NPs were localized in the tumor tissue in an upward trend as 2.27% (%ID/g) of the injected dose was detected in target tissue 120 minutes after injection. The three-fold growth of radioactivity in the solid tumor over time might be attributed to the receptor-mediated pathway in addition to enhanced permeability and retention (EPR) effect. Moreover, increasing of tumor-to-muscle uptake ratio (5.17–11.34 times) confirmed the tumor accumulation of radiolabeled NPs. Since the free gallium excretes mostly into the urine[52] and the renal system can excrete NPs <5.5 nm in hydrodynamic diameter,[51] a low accumulation of NPs in nontarget organs, especially in kidneys and bladder, can be related to high in vivo stability of ^{68}Ga-labeled NPs.

The sensitivity of MRI contrast agents is determined by their relaxivity. The higher relaxivity allows for contrast-enhanced MRI at the lower concentration of MR contrast agent. Relaxivity of DOTA–BN–TMC–MNPs was measured using MRI and obtained as 330.98 $mM^{-1}\cdot s^{-1}$. Feridex® (ferumoxides) and Resovist® (ferucarbotran) are MRI contrast media based on coated SPIONs approved as T_2- and T_2*-weighted MRI contrast agents for liver.

Relaxivity of ferumoxides and ferucarbotran was reported as 93 (87–99) and 143 (132–154) $mM^{-1}\cdot s^{-1}$ at 3T,[53] which is much less than DOTA–BN–TMC–MNPs' relaxivity (r_2=330.98 $mM^{-1}\cdot s^{-1}$). So DOTA–BN–TMC–MNPs can be utilized as a potential contrast enhancer in MRI.

DOTA–BN–TMC–MNPs were synthesized as PET/MR contrast media to visualize BC tumors in mice models, so the tumor uptake of NPs was evaluated by the MRI technique. Despite the lower sensitivity of MRI in comparison with PET imaging, iron concentration of DOTA–BN–TMC–MNPs was as sufficient as they can be detected by MRI in tumor lesion. The high accumulation of NPs in the liver obtained through MRI was very similar to the data observed from the biodistribution assay.

Subsequently, PET/CT imaging showed the apparent uptake of ^{68}Ga–DOTA–BN–TMC–MNPs in T-47D tumor inoculated into the right leg. Highly efficient ^{68}Ga labeling of DOTA–BN–TMC–MNPs and the high sensitivity of PET imaging led to a superior visibility of tumor by a lower concentration of NPs (0.62 mg/mL). There was a high accumulation of ^{68}Ga–DOTA–BN–TMC–MNPs in the liver as observed in biodistribution assay results and MRI. The SUV_{max} and SUV_{peak} ratios of tumor to the left leg (control) were calculated using PET/CT scans at 120 minutes and obtained as 19.6 and 15.4, respectively, indicating the meaningful uptake of ^{68}Ga–DOTA–BN–TMC–MNPs in tumor lesion. The tumor-to-liver ratio of maximum SUV was 0.178, associated with quick extraction of ^{68}Ga–DOTA–BN–TMC–MNPs in the hepatic first pass. Moreover, the ratios of tumor-to-muscle and tumor-to-liver uptake in the biodistribution assay were 11.34 and 0.197, which were correlated with PET/CT scan SUVs. It indicates that a simpler and less invasive estimation of biodistribution can provide using calculated SUVs of PET/CT scan.

Conclusion

Our findings demonstrated that BN conjugated to the surface-modified MNPs can be a promising agent for GRP receptor targeting. Small hydrodynamic size, low toxicity, highly efficient radiolabeling with ^{68}Ga, high serum stability, and strong binding affinity (IC_{50}=8.79 μg/mL) of DOTA–BN–TMC–MNPs toward GRP receptors make these NPs suitable for dual-modality PET/MRI of prostate, breast, and lung cancers.

Compliance with ethical standards

All animal experiments were performed in accordance with the ethical guidelines of Tehran University of Medical Sciences.

Acknowledgments

This research was a part of Maliheh Hajiramezanali's PhD thesis[54] (Department of Radiopharmacy, Faculty of Pharmacy, Tehran University of Medical Sciences, Tehran, Iran) and was supported by the International Atomic Energy Agency (IAEA; CRP Code: F22064) and the Tehran University of Medical Sciences (grant number 26985), Tehran, Iran. The authors would like to thank Ms Marzieh Ebrahimi and Mr Amin Mokhtari for their technical assistance.

Disclosure

The authors report no conflicts of interest in this work.

References

1. McNamara K, Tofail SAM. Nanoparticles in biomedical applications. *Adv Phys X*. 2017;2(1):54–88.
2. Ramos AP, Cruz MAE, Tovani CB, Ciancaglini P. Biomedical applications of nanotechnology. *Biophys Rev*. 2017;9(2):79–89. doi:10.1007/s12551-016-0246-2
3. Padmanabhan P, Kumar A, Kumar S, Chaudhary RK, Gulyás B. Nanoparticles in practice for molecular-imaging applications: an overview. *Acta Biomater*. 2016;41:1–16. doi:10.1016/j.actbio.2016.06.003
4. Leary JF, Key J. Nanoparticles for multimodal in vivo imaging in nanomedicine. *Int J Nanomedicine*. 2014;9:711–726. doi:10.2147/IJN.S53717
5. Yigit MV, Moore A, Medarova Z. Magnetic nanoparticles for cancer diagnosis and therapy. *Pharm Res*. 2012;29(5):1180–1188. doi:10.1007/s11095-012-0679-7
6. Sharifi S, Seyednejad H, Laurent S, Atyabi F, Saei AA, Mahmoudi M. Superparamagnetic iron oxide nanoparticles for *in vivo* molecular and cellular imaging. *Contrast Media Mol Imaging*. 2015;10(5):329–355. doi:10.1002/cmmi.1638
7. Laurent S, Bridot JL, Elst LV, Muller RN. Magnetic iron oxide nanoparticles for biomedical applications. *Future Med Chem*. 2010;2(3):427–449. doi:10.4155/fmc.09.164
8. Thomas R, Park IK, Jeong YY. Magnetic iron oxide nanoparticles for multimodal imaging and therapy of cancer. *Int J Mol Sci*. 2013;14(8):15910–15930. doi:10.3390/ijms140815910
9. Muthiah M, Park IK, Cho CS. Surface modification of iron oxide nanoparticles by biocompatible polymers for tissue imaging and targeting. *Biotechnol Adv*. 2013;31(8):1224–1236. doi:10.1016/j.biotechadv.2013.03.005
10. Yallapu MM, Foy SP, Jain TK, Labhasetwar V. PEG-functionalized magnetic nanoparticles for drug delivery and magnetic resonance imaging applications. *Pharm Res*. 2010;27(11):2283–2295. doi:10.1007/s11095-010-0260-1
11. Tekie FS, Kiani M, Zakerian A, et al. Nano polyelectrolyte complexes of carboxymethyl dextran and chitosan to improve chitosan-mediated delivery of miR-145. *Carbohydr Polym*. 2017;159:66–75. doi:10.1016/j.carbpol.2016.11.067
12. Naskar S, Koutsu K, Sharma S. Chitosan-based nanoparticles as drug delivery systems: a review on two decades of research. *J Drug Target*. 2018:1–15. doi:10.1080/1061186X.2018.1512112
13. Kulkarni AD, Patel HM, Surana SJ, Vanjari YH, Belgamwar VS, Pardeshi CV. N,N,N-Trimethyl chitosan: an advanced polymer with myriad of opportunities in nanomedicine. *Carbohydr Polym*. 2017;157:875–902. doi:10.1016/j.carbpol.2016.10.041
14. Abkar M, Fasihi-Ramandi M, Kooshki H, Lotfi AS. Oral immunization of mice with Omp31-loaded N-trimethyl chitosan nanoparticles induces high protection against brucella melitensis infection. *Int J Nanomedicine*. 2017;12:8769–8778. doi:10.2147/IJN.S149774
15. Paydary K, Seraj SM, Zadeh MZ, et al. The evolving role of FDG-PET/CT in the diagnosis, staging, and treatment of breast cancer. *Mol Imaging Biol*. 2018;21:1–10.

16. Rausch I, Quick HH, Cal-Gonzalez J, Sattler B, Boellaard R, Beyer T. Technical and instrumentational foundations of PET/MRI. *Eur J Radiol*. 2017;94:A3–A13. doi:10.1016/j.ejrad.2017.04.004
17. Ai F, Ferreira CA, Chen F, Cai W. Engineering of radiolabeled iron oxide nanoparticles for dual-modality imaging. *Wiley Interdiscip Rev Nanomed Nanobiotechnol*. 2016;8(4):619–630. doi:10.1002/wnan.1386
18. Lee CM, Jeong HJ, Cheong SJ, et al. Prostate cancer-targeted imaging using magnetofluorescent polymeric nanoparticles functionalized with bombesin. *Pharm Res*. 2010;27(4):712–721. doi:10.1007/s11095-010-0072-3
19. Laukkanen MO, Castellone MD. Gastrin-releasing peptide receptor targeting in cancer treatment: emerging signaling networks and therapeutic applications. *Curr Drug Targets*. 2016;17(5):508–614.
20. Morgat C, MacGrogan G, Brouste V, et al. Expression of gastrin-releasing peptide receptor in breast cancer and its association with pathologic, biologic, and clinical parameters: a study of 1,432 primary tumors. *J Nucl Med*. 2017;58(9):1401–1407. doi:10.2967/jnumed.116.188011
21. Spindel ER. Bombesin Peptides. In: Kastin AJ, editor. *Handbook of Biologically Active Peptides*. 2nd ed. San Diego: Academic Press; 2013:326–330. doi:10.1016/B978-0-12-385095-9.00046-4.
22. Ferreira CDA, Fuscaldi LL, Townsend DM, Rubello D, Barros ALBD. Radiolabeled bombesin derivatives for preclinical oncological imaging. *Biomed Pharmacother*. 2017;87:58–72. doi:10.1016/j.biopha.2016.12.083
23. Accardo A, Aloj L, Aurilio M, Morelli G, Tesauro D. Receptor binding peptides for target-selective delivery of nanoparticles encapsulated drugs. *Int J Nanomedicine*. 2014;9:1537–1557. doi:10.2147/IJN.S53593
24. Mu B, Liu P, Dong Y, Lu C, Wu X. Superparamagnetic pH-sensitive multilayer hybrid hollow microspheres for targeted controlled release. *J Polym Sci Part A Polym Chem*. 2010;48(14):3135–3144. doi:10.1002/pola.24095
25. Atyabi F, Majzoob S, Iman M, Salehi M, Dorkoosh F. In vitro evaluation and modification of pectinate gel beads containing trimethyl chitosan, as a multi-particulate system for delivery of water-soluble macromolecules to colon. *Carbohydr Polym*. 2005;61(1):39–51. doi:10.1016/j.carbpol.2005.02.005
26. Zhang J, Zhu X, Jin Y, Shan W, Huang Y. Mechanism study of cellular uptake and tight junction opening mediated by goblet cell-specific trimethyl chitosan nanoparticles. *Mol Pharm*. 2014;11(5):1520–1532. doi:10.1021/mp400685v
27. D'Huyvetter M, Aerts A, Xavier C, et al. Development of 177 Lu-nanobodies for radioimmunotherapy of HER2-positive breast cancer: evaluation of different bifunctional chelators. *Contrast Media Mol Imaging*. 2012;7(2):254–264. doi:10.1002/cmmi.491
28. Hamman JH, Kotzé AF. Effect of the type of base and number of reaction steps on the degree of quaternization and molecular weight of N-trimethyl chitosan chloride. *Drug Dev Ind Pharm*. 2001;27(5):373–380. doi:10.1081/DDC-100104312
29. Pardeshi CV, Belgamwar VS. Controlled synthesis of N, N, N-trimethyl chitosan for modulated bioadhesion and nasal membrane permeability. *Int J Biol Macromol*. 2016;82:933–944. doi:10.1016/j.ijbiomac.2015.11.012
30. Lie S. The EBC-ninhydrin method for determination of free alpha amino nitrogen. *J Inst Brew*. 1973;79(1):37–41. doi:10.1002/j.2050-0416.1973.tb03495.x
31. Liao N, Wu M, Pan F, et al. Poly (dopamine) coated superparamagnetic iron oxide nanocluster for noninvasive labeling, tracking, and targeted delivery of adipose tissue-derived stem cells. *Sci Rep*. 2016;6:18746. doi:10.1038/s41598-016-0001-8
32. Moon S-H, Yang BY, Kim YJ, et al. Development of a complementary PET/MR dual-modal imaging probe for targeting prostate-specific membrane antigen (PSMA). *Nanomedicine*. 2016;12(4):871–879. doi:10.1016/j.nano.2015.12.368
33. Nripen C, Shukla R, Katti KV, Raghuraman K. Gastrin releasing protein receptor – specific gold nanorods: breast and prostate tumor-avid nanovectors for molecular imaging. *Nano Lett*. 2009;9(5):1798–1805. doi:10.1021/nl8037147
34. Shirmardi SP, Gandomkar M, Mazidi M, Shafiei M, Maragheh MG. Synthesis and evaluation of a new bombesin analog labeled with Tc-99m as a GRP receptor imaging agent. *J Radioanal Nucl Chem*. 2011;288(2):327–335. doi:10.1007/s10967-011-0985-2
35. Sanjai C, Kothan S, Gonil P, Saesoo S, Sajomsang W. Superparamagnetic loaded nanoparticles based on biological macromolecules for in vivo targeted MR imaging. *Int J Biol Macromol*. 2016;86:233–241. doi:10.1016/j.ijbiomac.2016.01.049
36. Abu Elella MH, Mohamed RR, Abdel-Aziz MM, Sabaa MW. Green synthesis of antimicrobial and antitumor N,N,N-trimethyl chitosan chloride/poly (acrylic acid)/silver nanocomposites. *Int J Biol Macromol*. 2018;111:706–716. doi:10.1016/j.ijbiomac.2018.01.055
37. Thomas R, Park IK, Jeong YY. Magnetic iron oxide nanoparticles for multimodal imaging and therapy of cancer. *Int J Mol Sci*. 2013;14(8):15910–15930. doi:10.3390/ijms140815910
38. Ahmadi Lakalayeh G, Faridi-Majidi R, Saber R, Partoazar A, Mehr SE, Amani A. Investigating the parameters affecting the stability of superparamagnetic iron oxide-loaded nanoemulsion using artificial neural networks. *AAPS PharmSciTech*. 2012;13(4):1386–1395. doi:10.1208/s12249-012-9864-6
39. Boyer C, Whittaker MR, Bulmus V, Liu J, Davis TP. The design and utility of polymer-stabilized iron-oxide nanoparticles for nanomedicine applications. *NPG Asia Mater*. 2010;2(1):23–30. doi:10.1038/asiamat.2010.6
40. Mendoza-Sánchez AN, Ferro-Flores G, Ocampo-García BE, et al. Lys3-bombesin conjugated to 99mTc-labelled gold nanoparticles for in vivo gastrin releasing peptide-receptor imaging. *J Biomed Nanotechnol*. 2010;6(4):375–384.
41. Kulhari H, Pooja D, Singh MK, Kuncha M, Adams DJ, Sistla R. Bombesin-conjugated nanoparticles improve the cytotoxic efficacy of docetaxel against gastrin-releasing but androgen-independent prostate cancer. *Nanomedicine (Lond)*. 2015;10(18):2847–2859. doi:10.2217/nnm.15.107
42. Shukla S, Jadaun A, Arora V, Sinha RK, Biyani N, Jain VK. In vitro toxicity assessment of chitosan oligosaccharide coated iron oxide nanoparticles. *Toxicol Rep*. 2015;2:27–39. doi:10.1016/j.toxrep.2014.11.002
43. Arami H, Khandhar A, Liggitt D, Krishnan K. In vivo delivery, pharmacokinetics, biodistribution and toxicity of iron oxide nanoparticles. *Chem Soc Rev*. 2015;44(23):8576–8607. doi:10.1039/C5CS00541H
44. Clarke ET, Martell AE. Stabilities of the Fe(III), Ga(III) and In(III) chelates of N,N′,N″-triazacyclononanetriacetic acid. *Inorganica Chim Acta*. 1991;181(2):273–280. doi:10.1016/S0020-1693(00)86821-8
45. Clarke ET, Martell AE. Stabilities of trivalent metal ion complexes of the tetraacetate derivatives of 12-, 13- and 14-membered tetraazamacrocycles. *Inorganica Chim Acta*. 1991;190(1):37–46.
46. Shrivastava A, Ding H, Kothandaraman S, et al. A high-affinity near-infrared fluorescent probe to target bombesin receptors. *Mol Imaging Biol*. 2014;16(5):661–669. doi:10.1007/s11307-014-0727-2
47. Parry JJ, Andrews R, Rogers BE. MicroPET imaging of breast cancer using radiolabeled bombesin analogs targeting the gastrin-releasing peptide receptor. *Breast Cancer Res Treat*. 2007;101(2):175–183. doi:10.1007/s10549-006-9287-8
48. Gargosky SE, Wallace JC, Upton FM, Ballard FJ. C-terminal bombesin sequence requirements for binding and effects on protein synthesis in swiss 3T3 cells. *Biochem J*. 1987;247(2):427–432.
49. De Barros ALB, Das Graças Mota L, De Aguiar Ferreira C, et al. 99mTc-labeled bombesin analog for breast cancer identification. *J Radioanal Nucl Chem*. 2013;295(3):2083–2090. doi:10.1007/s10967-012-2331-8
50. Gustafson HH, Holt-Casper D, Grainger DW, Ghandehari H, Grainger D. Nanoparticle uptake: the phagocyte problem. *Nano Today*. 2015;10(4):487–510. doi:10.1016/j.nantod.2015.06.006

51. Wilhelm S, Tavares AJ, Dai Q, et al. Analysis of nanoparticle delivery to tumours. *Nat Rev Mater*. 2016;1(5):16014. doi:10.1038/natrevmats.2016.14
52. Autio A, Virtanen H, Tolvanen T, et al. Absorption, distribution and excretion of intravenously injected 68Ge/68Ga generator eluate in healthy rats, and estimation of human radiation dosimetry. *EJNMMI Res*. 2015;5(1):40. doi:10.1186/s13550-015-0083-5
53. Rohrer M, Bauer H, Mintorovitch J, Requardt M, Weinmann H-J. Comparison of magnetic properties of MRI contrast media solutions at different magnetic field strengths. *Invest Radiol*. 2005;40(11):715–724.
54. Hajiramezanali M. ^{68}*Ga-radiolabeled bombesin-conjugated to trimethyl chitosan-coated superparamagnetic nanoparticles for molecular imaging: preparation, characterization and biological evaluation* [PhD thesis]. Tehran: Tehran University of Medical Sciences; 2018.